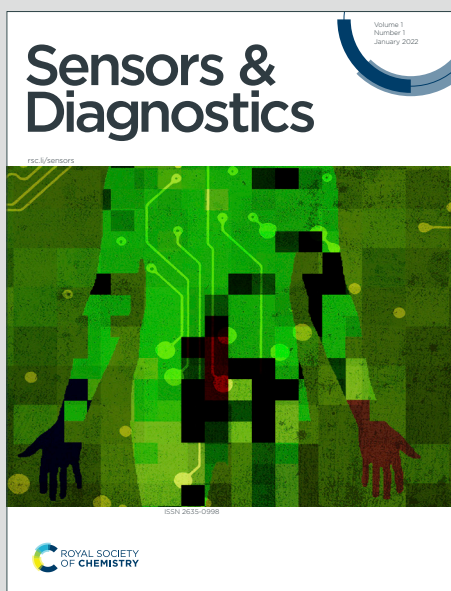


Sensors & Diagnostics

Accepted Manuscript

This article can be cited before page numbers have been issued, to do this please use: Y. Liu, C. Liu, Z. Dai and W. Guo, *Sens. Diagn.*, 2025, DOI: 10.1039/D5SD00236B.



This is an Accepted Manuscript, which has been through the Royal Society of Chemistry peer review process and has been accepted for publication.

Accepted Manuscripts are published online shortly after acceptance, before technical editing, formatting and proof reading. Using this free service, authors can make their results available to the community, in citable form, before we publish the edited article. We will replace this Accepted Manuscript with the edited and formatted Advance Article as soon as it is available.

You can find more information about Accepted Manuscripts in the [Information for Authors](#).

Please note that technical editing may introduce minor changes to the text and/or graphics, which may alter content. The journal's standard [Terms & Conditions](#) and the [Ethical guidelines](#) still apply. In no event shall the Royal Society of Chemistry be held responsible for any errors or omissions in this Accepted Manuscript or any consequences arising from the use of any information it contains.

Recent Advances in Multiplexed Electrochemiluminescence Immunoassays

Yu Liu,[†] Chunyan Liu,[†] Zhihui Dai,^{†, ‡, §} Weiliang Guo^{*, †, ‡}

[†]Collaborative Innovation Center of Biomedical Functional Materials, School of Chemistry and Materials Science, Nanjing Normal University, Nanjing 210023, China

[‡]State Key Laboratory of Analytical Chemistry for Life Science, Nanjing University, Nanjing 210023, China

[§]School of Chemistry and Molecular Engineering, Nanjing Tech University, Nanjing 211816, China

*Weiliang Guo, E-mail: guowl@njnu.edu.cn

Keywords Electrochemiluminescence; multiplex immunoassay; spectrum-resolved strategy; spatial-resolved strategy; protein biomarkers

Abstract Electrochemiluminescence (ECL) immunoassays have emerged as a powerful method for multiplex biomarker detection due to its advantages of low background noise, high sensitivity, and ease of miniaturization, holding significant applications in the precision medicine and in vitro diagnostics (IVD). This article systematically reviews recent advances in ECL-based multiplex immunoassays, focusing on two primary strategies for achieving multiplex detection. One is the spectrum-resolved strategy that enables differentiation of multiple targets by utilizing multicolor ECL luminophores, such as metal complexes and quantum dots, which emit light at distinct wavelengths. The other is the spatially resolved strategy that employs technologies including microarrays, microfluidic chips, and encoded microbeads to physically separate detection sites, allowing high-throughput analysis with just one luminophore. This review summarizes innovative designs under both strategies aimed at enhancing detection performance, discusses their applications in the diagnosis of diseases such as cancer and cardiovascular disorders, and addresses current challenges



related to analytical performance, system integration, and clinic use. Finally, prospects for ECL technology in IVD and precision medicine are outlined.

View Article Online
DOI: 10.1039/D5SD00236B

1. Introduction

Biomarkers are widely recognized as biochemical indicators of disease initiation and progression and therefore crucial for timely and precise diagnosis.^{1,2} However, conventional immunoassays are typically limited to measuring only one biomarker at a time (termed as single-plex immunoassays). The quantification of biomarkers always depends on a single readout signal, rendering the results susceptible to the environmental interference, and consequently resulting in false-positive or false-negative errors.^{3,4} In contrast, multiplex immunoassays can measure multiple biomarkers in a single run and significantly improve diagnostic accuracy and efficiency. Moreover, it offers higher detection throughput, lower sample consumption, and reduced assay costs.⁵ Therefore, multiplex immunoassays have garnered widespread attention in clinical bioanalysis.^{6,7}

In recent years, numerous efforts have focused on developing novel multiplex immunoassays by integrating techniques such as radioisotopic,⁸ optical,^{9–11} spectroscopic,¹² and electrochemical methods.¹³ Electrochemiluminescence (ECL) refers to a light-emitting process in which the excited-state species is generated via high energy electron transfer reactions at the electrode surface.^{14–16} In comparison with the methods that rely on the external light excitation such as fluorescence and surface plasmon resonance, ECL reactions do not require an external light source for excitation, thus avoiding the interference from light scattering and offering outstanding advantages of high detection sensitivity and near-zero background.¹⁷ When compared with chemiluminescence that takes place in a mixed solution, ECL reactions occur near the electrode surface and are highly sensitive to interfacial processes, exhibiting excellent spatiotemporal control.¹⁸

A wide variety of ECL luminophores, ranging from aromatic hydrocarbons and metal complexes to nanomaterials, have been synthesized.^{19–21} However, tris(2,2'-bipyridyl)ruthenium(II) ($\text{Ru}(\text{bpy})_3^{2+}$) remains the most extensively employed in



fundamental studies. In the presence of tri-*n*-propylamine (TPrA) as the coreactant, Ru(bpy)₃²⁺ exhibits high and stable ECL emission in aqueous solutions, thus making ECL as one of the most powerful commercial analytical techniques.^{14,22} For instance, over 100 distinct biomarkers (e.g., cancer, inflammatory, or cardiac biomarkers, as well as hormones) can be determined based on based on the ECL immunoassay devices commercialized by Roche Diagnostics and Meso Scale Discovery (MSD).

This review offers a comprehensive overview of ECL immunoassays, designed specifically for researchers new to the field. We begin with a brief introduction to the fundamental principles of ECL, followed by a summary of recent progress in both spectral and spatial-resolved strategies for constructing multiplexed ECL immunoassays. Key achievements in enhancing analytical performance are also highlighted. Finally, we discuss the current challenges and future perspectives for the advancement of ECL immunoassays.

2. Fundamentals of ECL

2.1 Annihilation Pathway

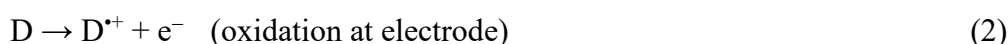
The annihilation pathway represents one of the earliest elucidated and most classical mechanisms for ECL generation. Early detailed studies of annihilation ECL focused primarily on polycyclic aromatic hydrocarbons such as rubrene and 9,10-diphenylanthracene (DPA), as well as metal complexes like tris(bipyridine)ruthenium(II) (Ru(bpy)₃²⁺).²³ In this scheme, the oxidized and reduced species are typically generated sequentially at two different electrode potentials, followed by electron transfer between these species to produce an excited state.²⁴

In general, the annihilation mechanism can be summarized as follows. The potential of the working electrode is switched rapidly between two values. At the cathode, luminophore A is reduced to A⁻ (eq 1), while at the anode, luminophore D is oxidized to D⁺ (eq 2). These two species annihilate near the electrode surface to generate the excited-state species A* (eq 3), which then emits light (eq 4). Depending on the identity of the reactants, the process is classified as “homogeneous annihilation” (A and D are



the same species) or “heterogeneous annihilation” (A and D are different species).^{25,26}

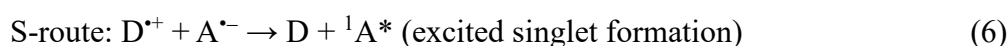
For example, in the homogeneous annihilation of Ru(bpy)₃²⁺, oxidized Ru(bpy)₃³⁺ and reduced Ru(bpy)₃⁺ react to produce the excited state Ru(bpy)₃^{2+*} with concomitant light emission. A representative heterogeneous annihilation is the cross-reaction between the DPA anion radical and the *N,N,N',N'*-tetramethyl-*p*-phenylenediamine (TMPD) cation radical.²⁷



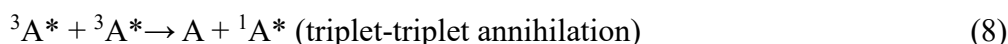
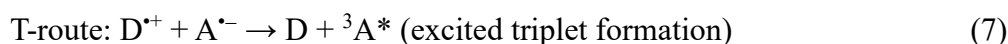
Depending on the relationship between the reaction enthalpy change and the excited state energy (eq 5), where $-\Delta H_{\text{ann}}$ is the enthalpy of ion annihilation and E_P is the peak potential for electrochemical oxidation or reduction, the annihilation pathway can be further classified into the singlet-state route (S-route) and the triplet-state route (T-route).²⁸

$$-\Delta H_{\text{ann}} = E_P(D^{\cdot+}/D) - E_P(A/A^{\cdot-}) - 0.157 \quad (5)$$

When $-\Delta H_{\text{ann}} > E_S$, the system is energy-sufficient and follows the S-route, directly producing the singlet excited state ¹A* (eq 6), which then emits light, as observed in the DPA annihilation system.^{29,30}



When $-\Delta H_{\text{ann}} < E_S$, the system is energy-deficient and follows the T-route. Here, the triplet excited state ³A* is initially formed (eq 7), followed by its conversion to ¹A* via triplet-triplet annihilation (eq 8), as exemplified by the TMPD^{•+}/DPA^{•-} system.³¹



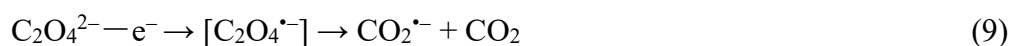
2.2 Coreactant Pathway

While the annihilation pathway represents a milestone in elucidating the fundamental principles of ECL, the reliance on non-aqueous solvents restricts its application in bioanalysis. In contrast, the coreactant pathway plays a crucial role in commercial ECL



immunoassays due to its exceptional efficiency and compatibility in aqueous media. In this case, the use of a coreactant can significantly enhance the ECL generation from the luminophore. Based on the electrochemical processes occurring near the electrode and the types of active intermediates generated, the coreactant mechanisms can be accordingly categorized into two main pathways, namely “oxidative-reduction” and “reductive-oxidation”.³²

Oxidative-reductive coreactants generate strong reducing intermediates upon electrochemical oxidation, which then reduce the oxidized luminophore to form the excited state. This type of coreactant is the most widely used, with typical examples including oxalate ion ($C_2O_4^{2-}$) and TPrA. Oxalate, the first discovered coreactant, undergoes bond cleavage under anodic oxidation conditions to produce the strongly reducing $CO_2^{\cdot-}$ (eq 9). Simultaneously, the luminophore $Ru(bpy)_3^{2+}$ is oxidized to $Ru(bpy)_3^{3+}$ (eq 10). Subsequently, $CO_2^{\cdot-}$ reduces $Ru(bpy)_3^{3+}$ to the excited state $Ru(bpy)_3^{2+*}$ (eq 11), which then emits light (eq 12).²²



TPrA, as the coreactant in commercial ECL systems, exhibits a more complex oxidation process involving multiple parallel reaction pathways.^{33,34} Initially, TPrA undergoes electrochemical oxidation at the electrode surface to form the radical cation $TPrA^{\cdot+}$ (eq 13), which rapidly undergoes deprotonation to yield the strongly reducing intermediate $TPrA^{\cdot}$ (eq 14).³⁵



Figure 1 summarizes several proposed reaction mechanisms. For instance, this reducing intermediate can directly reduce $Ru(bpy)_3^{3+}$ to generate the excited state (**Figure 1a**). Simultaneously, $TPrA^{\cdot}$ can also reduce $Ru(bpy)_3^{2+}$ to $Ru(bpy)_3^{\cdot+}$, which subsequently undergoes an annihilation reaction with $Ru(bpy)_3^{3+}$ to produce light emission (**Figure 1b**). **Figure 1c** illustrates the generation of the excited state



$\text{Ru}(\text{bpy})_3^{2+}$ via the so-called low oxidation potential pathway, where only TPrA, but not $\text{Ru}(\text{bpy})_3^{2+}$, undergoes electrochemical oxidation. In contrast, in the catalytic pathway TPrA^{•+} and TPrA[•] are generated via homogeneous oxidation between electrogenerated $\text{Ru}(\text{bpy})_3^{3+}$ and TPrA, rather than through the direct electrochemical oxidation of TPrA at the electrode surface (**Figure 1d**). Notably, this pathway is favored when the concentration of $\text{Ru}(\text{bpy})_3^{2+}$ is high.³⁶

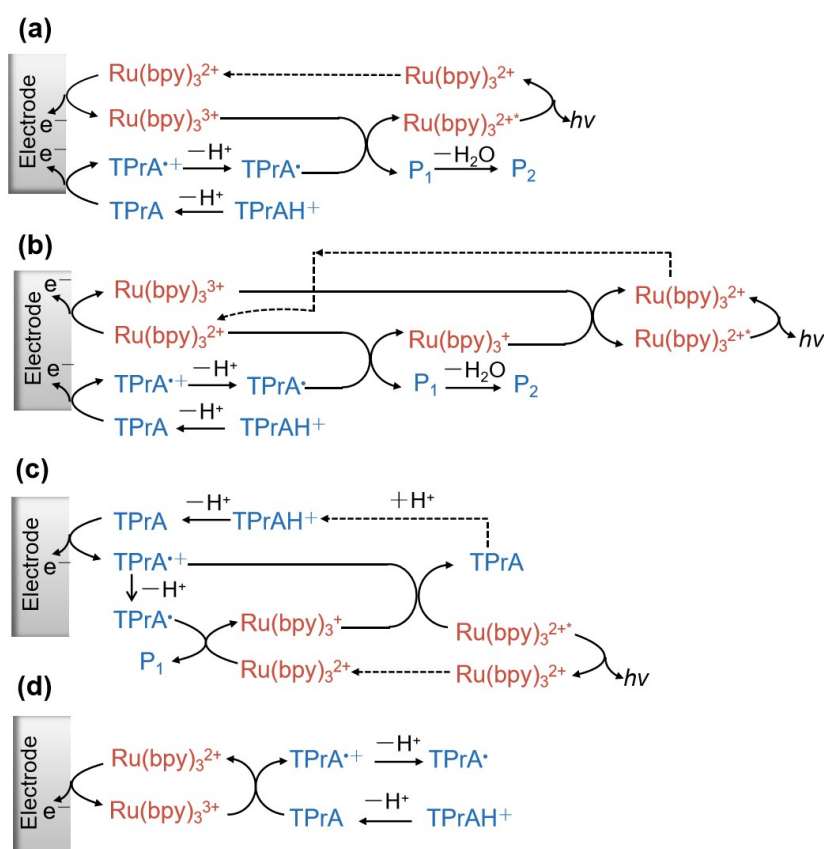


Figure 1. Proposed mechanism for $\text{Ru}(\text{bpy})_3^{2+}/\text{TPrA}$ ECL excited state formation and light emission.

Reductive-oxidative coreactants generate strong oxidizing intermediates upon electrochemical reduction, which then oxidize the reduced luminophore to yield the excited state. A typical example is peroxydisulfate ($\text{S}_2\text{O}_8^{2-}$), which undergoes cathodic reduction to generate $\text{SO}_4^{\cdot-}$ (eq 15), possessing an extremely high oxidation potential (3.15 V vs SCE). $\text{Ru}(\text{bpy})_3^{2+}$ is first reduced to $\text{Ru}(\text{bpy})_3^+$ (eq 16) and is subsequently oxidized by $\text{SO}_4^{\cdot-}$ to the emissive excited state (eq 17).³⁷





At present, a deeper understanding of ECL mechanisms has been achieved, facilitated by various advanced techniques including optical microscopy, mass spectrometry, and spectroscopic measurement. For example, electrochemistry coupled mass spectrometry (ECMS) enables the capture and identification of short-lived intermediates (e.g., radical cation TPrA^{•+}, neutral radical TPrA[•]) involved in ECL reactions, providing direct evidence for coreactant pathways and transforming previously proposed ECL mechanisms into experimentally validated findings.^{38,39} Furthermore, both ECL-based microscopy (ECLM) and ECL self-interference spectroscopy (ECLIS) allow the observation of the spatial distribution of ECL-emitting layer, and have been employed to decipher ECL reaction mechanisms. By measuring the thickness of the emission layer, the switch of the dominant ECL pathway can be resolved and regulated via the luminophore concentration or the concentration ratio of luminophore to coreactant.^{40–42}

3. Strategies for Multiplexed ECL Detection

3.1 Spectrum-Resolved Strategy

Spectrum-resolved multiplexed ECL immunoassay represents a significant technological advancement beyond conventional single-analyte detection. It involves constructing specific molecular luminophores through the integration of biological recognition units and ECL luminophores with distinguishable emission wavelengths, thereby allowing for the simultaneous, high-throughput detection of multiple analytes in complex biological samples. The exploration of spectral resolution strategies begins with the use of structurally well-defined metal complexes. Richter characterized the spectral properties of inorganic metal complexes including Ru(bpy)₃²⁺ derivatives, Os(phen)₂(dppene)²⁺ (phen = 1,10-phenanthroline, dppene = cis-1,2-bis(diphenylphosphino)ethylene), and Ir(ppy)₃ (ppy = 2-phenylpyridine). By judicious



modification of ligands with bipyridine and phenanthroline derivatives, emission wavelengths were precisely tuned across the 500–700 nm range, yielding a versatile luminophore panel spanning blue, green, and red spectral regions.^{43,44} The studies have paved the way for achieving multiplex detection in spectrum-resolved ECL immunoassays.

In spectrum-resolved multiplex ECL immunoassays, the spectral characteristics of the luminophores directly determine the number of targets that can be simultaneously detected. While molecular luminophores always exhibit broad full-width at half-maximum, resulting in the heavy spectral overlap, and thus restricting the multiplexing capacity of spectrum-resolved ECL immunoassays. Su et al. developed a potential-modulated spectrum-resolved strategies based on novel ruthenium(II) and iridium(III) complexes, thus constructing a dual-resolved ECL system for multiplex immunoassays (**Figure 2a**). They synthesized $\text{Ru}(\text{bpy})_2(\text{dvbpy})^{2+}$ ($\text{bpy} = 2,2'$ -bipyridine, $\text{dvbpy} = 4,4'$ -bis(4-vinylphenyl)-2,2'-bipyridine, $\lambda_{\text{max}} = 636 \text{ nm}$) and $\text{Ir}(\text{dFCF}_3\text{ppy})_2(\text{dtbbpy})^+$ ($\text{dFCF}_3\text{ppy} = 3,5$ -difluoro-2-[5-(trifluoromethyl)-2-pyridinyl]-phenyl, $\text{dtbbpy} = 4,4'$ -bis(tert-butyl)-2,2'-bipyridine, $\lambda_{\text{max}} = 491 \text{ nm}$), achieving a 145 nm spectral separation, and further realized potential-regulated switch on/off emission of $\text{Ir}(\text{ppy})_3$ ($\lambda_{\text{max}} = 526 \text{ nm}$), thus allowing for the potential-resolved ECL emission. As illustrated in **Figure 2b**, applying sequential potentials at +0.74 V, +1.33 V, and +1.75 V selectively activated each luminophore, enabling both spectral and potential resolution. Building on this principle, these three luminophores were loaded into polystyrene beads to encode detection antibodies for carcinoembryonic antigen (CEA), alpha-fetoprotein (AFP), and beta-human chorionic gonadotropin (β -hCG). This ultimately enabled the simultaneous identification of all three cancer markers in a single sample and scan.⁴⁵

View Article Online
DOI: 10.1039/D5SD00236B



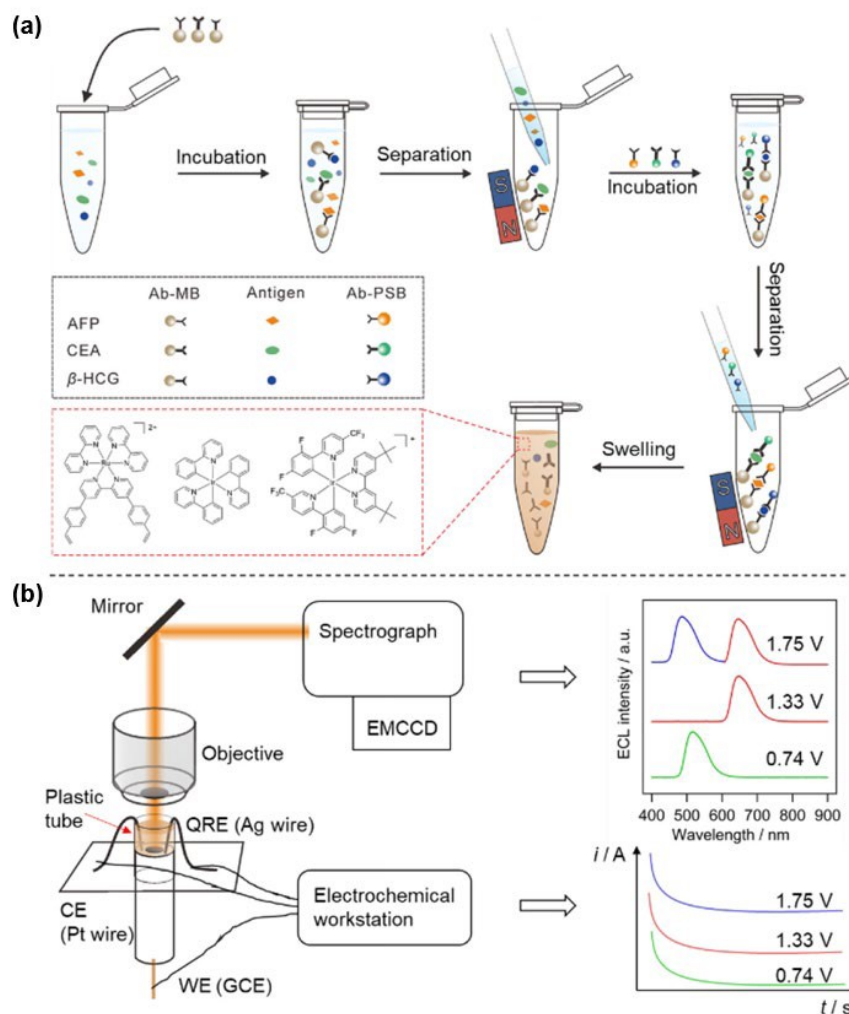


Figure 2. Potential-resolved and spectrum-resolved ECL strategy for multiplex immunoassay. (a) Schematic procedure for the simultaneous detection of three tumor markers. (b) ECL detection platform and the principle of selectively activating three luminophores at different applied potentials. Reprinted with permission from Ref 45. Copyright 2018 American Chemical Society.

Quantum dots (QDs) demonstrate the theoretical capability for simultaneous discrimination of four to five or even more targets, owing to their extremely narrow emission peaks, tunable wavelengths, and co-excitation capacity. As one of the earliest labeling materials applied in spectrum-resolved ECL immunoassays, QDs exhibit emission spectra covering the visible, near-infrared, and even far-infrared regions.⁴⁶ This excellent spectral tunability provides a crucial material foundation for the development of ECL-based multiplex detection strategies. Miao et al. developed dual-



stabilizers-capped CdSe ($\lambda_{\max} = 550$ nm) and CdTe ($\lambda_{\max} = 776$ nm) nanocrystals as ECL labels for the simultaneous detection of AFP and CEA, with the limit of detection (LOD) of 10 fg/mL and 1 pg/mL, respectively. Using ammonium persulfate ((NH₄)₂S₂O₈) as a cathodic ECL coreactant, the ECL signal was generated during cathodic potential scanning. The resulting ECL spectra from the two immobilized luminophores effectively eliminated cross-talk, thereby overcoming the spectral overlap inherent in traditional multiplex ECL assays.⁴⁷

Furthermore, Zou et. al reported the spectrally resolved three-color ECL multiplex immunoassay. Firstly, they synthesized dual-stabilizers-capped CdSe ($\lambda_{\max} = 550$ nm), CdTe ($\lambda_{\max} = 650$ nm), and CdTe ($\lambda_{\max} = 776$ nm) nanocrystals. By applying a potential in a buffer containing (NH₄)₂S₂O₈ and collecting emission intensities across wavelengths via a spectrometer, they successfully achieved simultaneous detection of three tumor markers, namely CEA, prostate-specific antigen (PSA), and AFP, on a single electrode interface, with LOD of 1, 10, and 0.01 pg/mL, respectively. With the ongoing development of new monochromatic ECL luminophores covering broader spectral ranges, this strategy could potentially be extended to detect four or more targets simultaneously.⁴⁸

To fundamentally solve the problems of low efficiency and poor stability of conventional QDs, innovative core/shell/shell structures (CdSe core-CdS intermediate layer-ZnS outer layer) were developed by Su and coworkers. These QDs maintained near-unity photoluminescence quantum yields (>90%) and narrow emission peaks in aqueous solution. Their ECL efficiency was enhanced by six orders of magnitude compared to the conventional Ru(bpy)₃²⁺ emitter, and the relative standard deviation of the luminescence intensity remained below 1% over 125 consecutive potential scan cycles, demonstrating excellent operational stability. They precisely controlled the CdSe core size to prepare three-color quantum dots emitting at 549 nm (green), 592 nm (yellow), and 643 nm (red), with emission wavelength intervals of approximately 50 nm (**Figure 3a**). As illustrated in **Figure 3b**, by mixing these luminophores in a phosphate-buffered solution containing K₂S₂O₈ and applying a cathodic potential sweep (−0.9 V to −1.3 V) on a single working electrode, the ECL emissions of the



different QDs could be sequentially and selectively excited. The resulting signals were spectrally well-resolved with negligible crosstalk (**Figure 3c–e**), providing a practical strategy for high-throughput detection of multiple biomarkers.⁴⁹

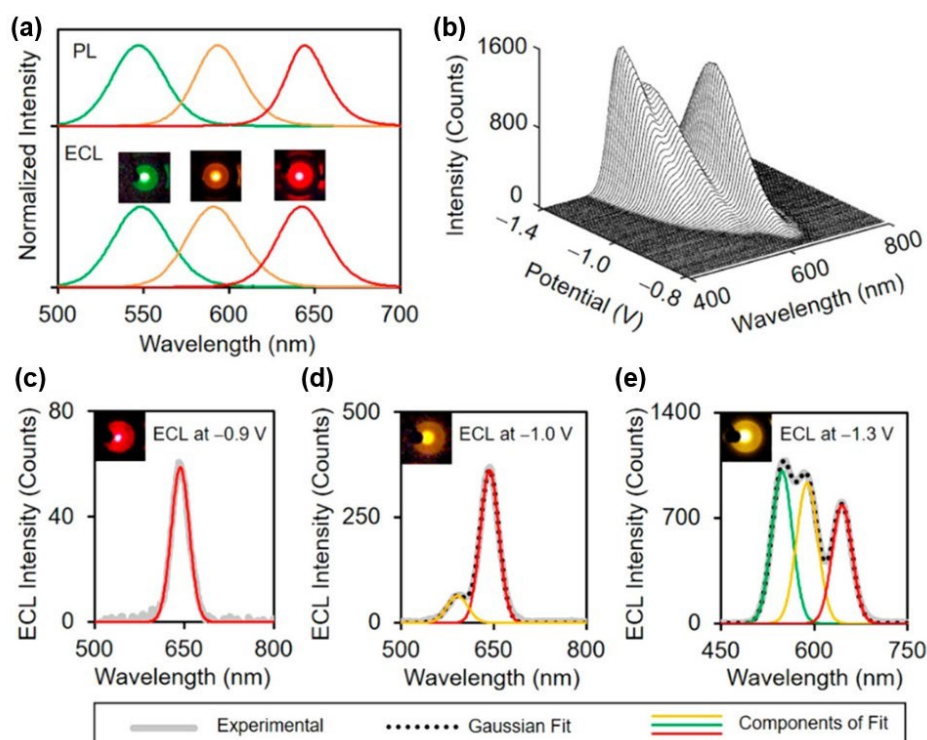


Figure 3. (a) Normalized PL spectra and ECL photographs of green-, yellow-, and red-emitting CdSe/CdS/ZnS Core/Shell/Shell QDs. (b) ECL-potential spectra of a mixed solution containing the three colors of QDs. (c–e) ECL spectra and corresponding photographs (insets) of the three-component mixed system at three different applied potentials. Reprinted with permission from Ref 49. Copyright 2020 American Chemical Society.

Due to the restricted spectral range of the visible region (400–750 nm), spectral multiplexing is constrained by the limited number of resolvable channels. The development of near-infrared (NIR) luminophores can extend the detectable spectral window, thereby increasing the number of resolvable channels for multiplex detection. Moreover, the NIR luminophores offer the minimal autofluorescence, significantly reducing background noise and thus enhancing the signal-to-noise ratio compared to



conventional UV-visible detection. However, most aqueous NIR ECL luminophores, such as graphene oxide and CdTe QDs, typically emit below 800 nm and suffer from substantial spectral overlap in multiplexed detection, compromising both sensitivity and accuracy. To address this issue, Shen et al. reported the fabrication of an innovative NIR ECL luminophore based on bovine serum albumin-stabilized silver nanoclusters (BSA-Ag NCs). When coupled with TiO₂ nanoparticles as a coreactant accelerator, the luminophore enabled highly efficient anodic ECL emission at 904 nm in aqueous medium to surpass the 900 nm threshold. By tagging anti-cancer antigen 125 (anti-CA125), anti-carbohydrate antigen 19-9 (anti-CA19-9) and anti-cardiac troponin I (anti-cTnI) secondary antibodies with CdSe NCs (λ_{\max} = 553 nm), CdTe NCs (λ_{\max} = 676 nm) and the new BSA-Ag NCs (λ_{\max} = 904 nm), respectively, they achieved three baseline-resolved emission peaks in a single potential sweep, thus demonstrating a three-color, spectrally resolved ECL multiplex immunoassay on a single electrode surface (**Figure 4a**).⁵⁰

Spectrum-resolved measurement using spectrometers often suffers from sensitivity loss due to the slits in the monochromator. Photomultiplier tubes (PMTs), by contrast, provide highly sensitive detection and enable spectral resolution without sensitivity trade-off, when combined with optical filters. Zou et al. achieved spectrally resolved multiplexed ECL detection by combining two PMTs with a dichroic mirror. ECL emission from two QDs, namely, CdSe (550 nm) and CdTe (790 nm) were completely separated by the dichroic mirror and measured by two PMTs, respectively. As a result, this dual-band ECL detection platform exhibited LOD of 1 pg/mL for AFP and 1 mU/mL for CA125, avoiding the spectral overlap and improving detection sensitivity.⁵¹ Very recently, Shen et al. reported a potential and spectrum dual-resolved ECL immunoassay based on a custom three-channel bandpass filter wheel (**Figure 4b**). In a single cathodic sweep, perylene tetracarboxylic acid@carboxylic carbon nanotubes (710 nm) were first activated at lower potentials (0–0.8 V) for AFP detection. After rotating the filter wheel, CdSe (550 nm) and CdTe (750 nm) quantum dots were sequentially read out for spectral-resolved detection of CA125 and CA19-9. The assay



achieved detection limits of 0.53 fg/mL, 0.058 mU/mL, and 0.11 mU/mL for AFP, CA125, and CA19-9, respectively, which matched well with the performance of single-plex immunoassays. This platform eliminates the need for spectrometers and offers a low-cost and high-throughput ECL detection.⁵²

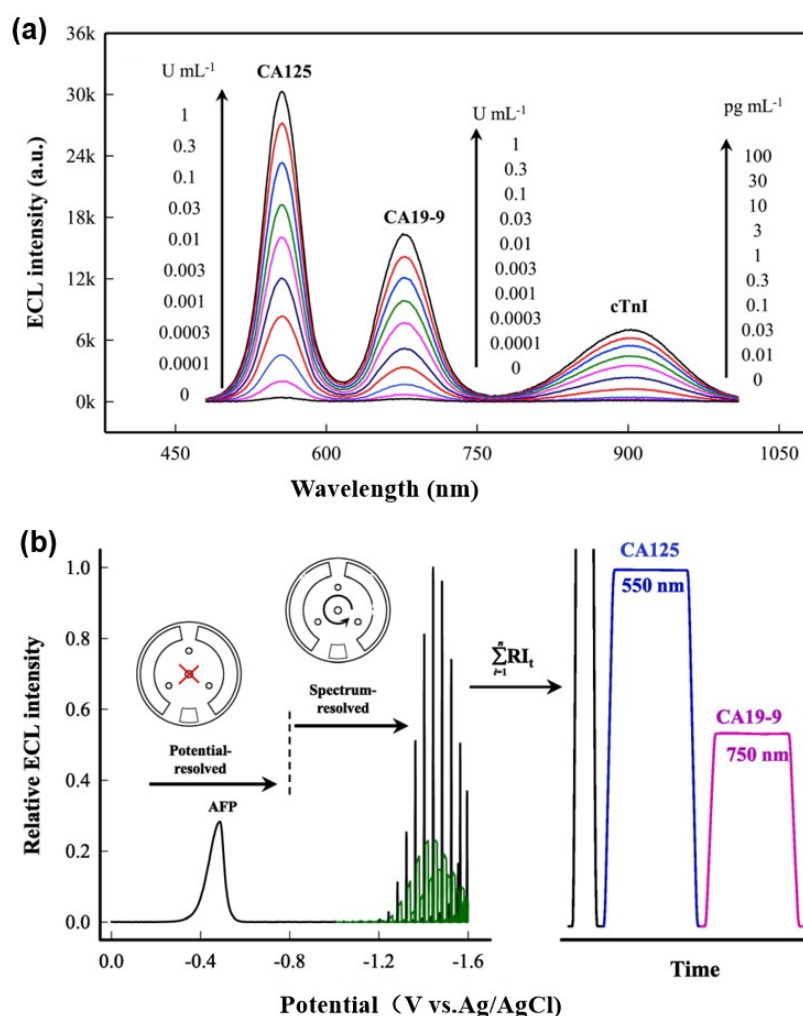


Figure 4. (a) Spectrum-resolved ECL MIA toward samples containing CA125, CA19-9 and cTnI at different concentrations. Adapted with permission from Ref⁵⁰. Copyright 2020 Elsevier B.V. (b) Schematic illustration of the potential- and spectrum-resolved dual-mode ECL measurement process for the simultaneous detection of AFP, CA125, and CA19-9. Adapted with permission from Ref 52. Copyright 2024 Elsevier B.V.



In addition to the metal complexed and quantum dots discussed above, a variety of other materials have been synthesized for spectrum-resolved ECL immunoassays. For instance, metal-free carbon-based nanomaterials have attracted considerable attention due to their good biocompatibility and tunable photoelectric properties.⁵³ **Table 1** summarized the recent advances in spectrum-resolved multiplex ECL immunoassays employing various luminophores. The analytical performance of these assays, including limit of detection and linear ranges, is also compared.



Table 1. Summary of spectrum-resolved ECL multiplex immunoassays, including ECL luminophores and emission wavelengths, target biomarkers, limit of detection, and linear ranges.

No.	ECL luminophores & $\lambda_{em\ max}$	Targets	Limit of Detection	Liner range	Ref
1	CdSe QDs; 550 nm	AFP	10 fg/mL	50–1.0×10 ⁵ fg/mL	47
	CdTe QDs; 776 nm	CEA	1 pg/mL	10–1.0×10 ⁴ pg/mL	
2	CdSe QDs; 550 nm	CEA	1.0 pg/mL	0.01–10 ng/mL	48
	CdTe QDs; 650 nm	PSA	10.0 pg/mL	0.1–100 ng/mL	
	CdTe QDs; 776 nm	AFP	0.01 pg/mL	0.1–100 pg/mL	
3	CdSe QDs; 553 nm	CA125	0.035 mU/mL	0.1–1.0×10 ³ mU/mL	50
	CdTe QDs; 676 nm	CA19-9	0.087 mU/mL	0.3–1.0×10 ³ mU/mL	
	BSA-Ag NCs; 904 nm	cTnI	0.016 pg/mL	0.03–100 pg/mL	
4	CdSe QDs; 550 nm	AFP	1 pg/mL	5–5.0×10 ³ pg/mL	51
	CdTe QDs; 790 nm	CA125	1 mU/mL	5–1.0×10 ³ mU/mL	
5	CdSe QDs; 550 nm	CA125	0.058 mU/mL	0.1–300 mU/mL	52
	CdTe QDs; 750 nm	CA19-9	0.11 mU/mL	0.3–300 mU/mL	
	PTCA@CNTs; 710 nm	AFP	0.53 fg/mL	0.003–10 pg/mL	
6	CNNs; 438 nm	CA19-9	0.083 U/mL	0.01–80 U/mL	53
	S-CNNS; 510 nm	Mesothelin	0.91 ng/mL	0.001–50 µg/mL	
7	Zn-AIE-AuNCs; 485 nm	CEA	0.3 pg/mL	1.0–5×10 ⁴ pg/mL	54
	CIS@ZnS nanocrystals; 775 nm	P53	0.5 pM	1.0–5×10 ⁴ pM	



3.2. Spatial-Resolved Strategy

View Article Online
DOI: 10.1039/D5SD00236B

Beyond the spectrum-resolved strategy, the spatially resolved strategy offers a promising alternative for achieving multiplexed immunoassays in a single run, when combined with the ECL imaging technology.⁵⁵ This strategy mainly lies in physically separating capture antibodies for different analytes onto independent, addressable spatial locations or carriers, enabling multiplexed detection using only a single and universal ECL luminophore. It exhibits three remarkable advantages, (i) it avoids spectral overlap and signal crosstalk caused by multiple luminophores. (ii) It reduces system complexity by eliminating the need to optimize specific labels and detection conditions for each analyte. (iii) It can overcome the throughput limitations imposed by spectral channels, because the multiplexing capacity depends on the number of precisely encoded spatial addresses. Therefore, this strategy serves as a straightforward and reliable means of expanding the multiplexing capacity of ECL immunoassays.⁵⁶

Microarrays are commonly used substrates for immobilizing different capture antibodies at defined locations, thus achieving spatial separation of detection sites. A typical example is the work reported by Pfeifer et al., who constructed 50 spatially separated detection spots on a 4 mm diameter electrode (**Figure 5a-c**), allowing for the simultaneous determination of two triplex biomarker panels for traumatic brain injury and cardiac diseases, and achieving detection limits of 1–33 pg/mL with good reproducibility and specificity (cross-reactivity <6%).⁵⁷ In addition, a triple ECL detection array was constructed by the combined use of disposable screen-printed carbon electrodes and a portable ECL reader, which enables the simultaneous detection of three biomarkers, namely GFAP, h-FABP, and S100 β , without the cross-reactivity. In comparison with the conventional imaging techniques such as CT and MRI, this approach offers advantages including simple operation, fast detection, and low cost, making it particularly suitable for resource-limited environments such as accident sites and remote areas.⁵⁸

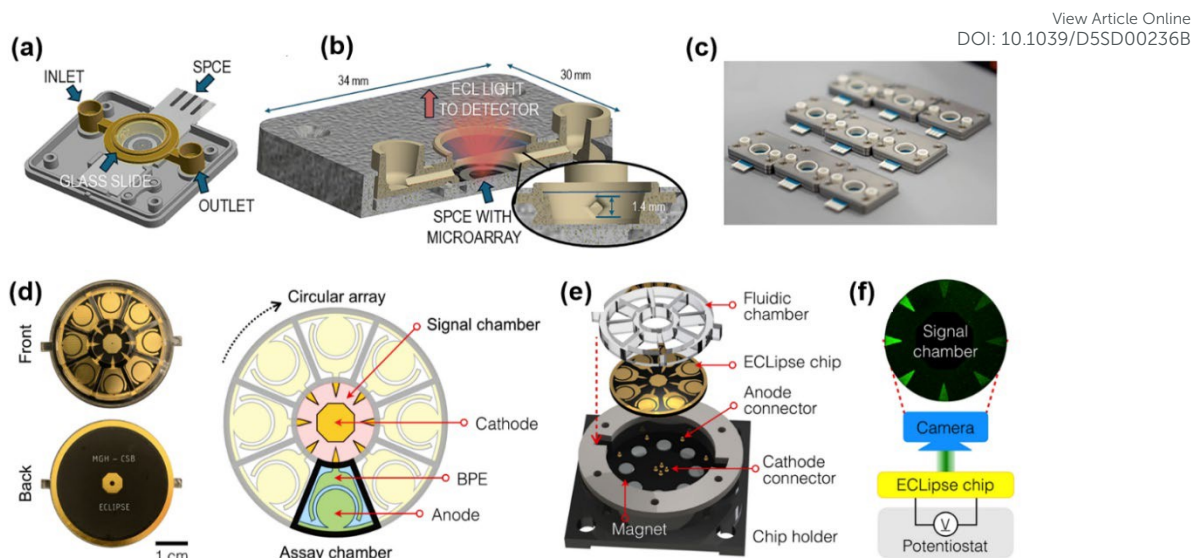
The aforementioned works usually employed nano-spotting or 3D printing to precisely immobilizing or spatially separating capture antibodies on the substrate electrode. Alternatively, Cui et al. reported a different approach based on a single-



electrode configuration for microarray fabrication, achieving the simultaneous quantitative detection of acute myocardial infarction (AMI) biomarkers, such as cTnI, h-FABP, and copeptin. Validation with 260 clinical serum samples demonstrated 100% sensitivity and specificity, significantly surpassing the conventional high-sensitivity cardiac troponin T (hs-cTnT) assay, and reducing the misdiagnosis rate by over 20% within the critical 3–12 hour window after symptom onset. It thus provides a reliable measurement tool for the early and accurate diagnosis of AMI.⁵⁹

Furthermore, microfluidic chips enable automated sample and reagent delivery, making them a popular platform for multiplexed ECL immunoassays. Rusling and coworkers fabricated a monolithic 3D-printed microfluidic chip integrated with an automated micro-pump controller. The assay can complete the simultaneous detection of eight prostate cancer biomarkers in human serum in only 25 minutes, with detection limits as low as 78–110 fg/mL, providing a powerful tool for rapid clinical multi-parameter diagnosis.⁶⁰ As illustrated in **Figure 5d-f**, a novel sensing system termed ECLipse (ECL in paired signal electrode) chip was constructed, in which the biorecognition and ECL generation processes were physically separated via bipolar electrodes (BPEs). In this modular design, the triangular tips of eight BPEs were positioned within a single signal chamber containing ECL luminophores, while biorecognition reactions occurred in eight independent assay chambers, thus allowing for the simultaneous detection of eight targets in a single run. Meanwhile, this chip achieved detection limits of 15–230 fg/mL and an over 7000-fold increase in detection sensitivity compared to conventional ELISA.⁶¹





View Article Online
DOI: 10.1039/D5SD00236B

Figure 5. (a) Schematic illustration of the disposable microfluidic cartridge and fluidic channel design. (b) Photograph of the cartridge held in hand. (c) Photograph of the cartridge loaded into the drawer of the ECL reader prior to measurement. Reprinted with permission from Ref 57. Copyright 2022 American Association for the Advancement of Science. (d) Electrode layout with an eight-channel circular array, common cathode, signal chamber, and assay chamber. (e) Chip assembly: plastic fluidic layer bonded to PCB, integrated magnet array, and pogo pins for electrical connection. (f) Signal detection: applied potential drives ECL reaction in the signal chamber for real-time imaging by a CCD camera. Reprinted with permission from Ref 61. Copyright 2022 American Association for the Advancement of Science.

In contrast to planar microarrays or microfluidic chips that rely on precisely patterned electrodes or physically isolated channels to achieve spatial resolution, spot-free microbead-based arrays offer a fundamentally different and highly versatile approach for multiplexed ECL immunoassays. Rather than immobilizing capture antibodies on predefined two-dimensional substrates, microbeads function as addressable carriers for antibody immobilization. By encoding microbeads with fluorescent dyes, shapes, or diameters, bead-based ECL immunoassays can achieve high-order multiplexing. As shown in **Figure 6a**, Sojic and Walt demonstrated a bead-based microarray that combines fluorescent encoding with single-bead ECL imaging.



Fluorescent encoding was achieved by doping beads with varying Eu^{3+} dye concentrations and conjugating them to specific capture antibodies, allowing each bead to be identified by its characteristic fluorescence intensity. After loaded onto a gold-coated optical fiber bundle electrode microwell array, the encoded beads were subjected to a sandwich immunoassay using an ECL luminophore (SA-Ru complex), ultimately enabling spatially resolved ECL imaging at the single-bead level.⁶²

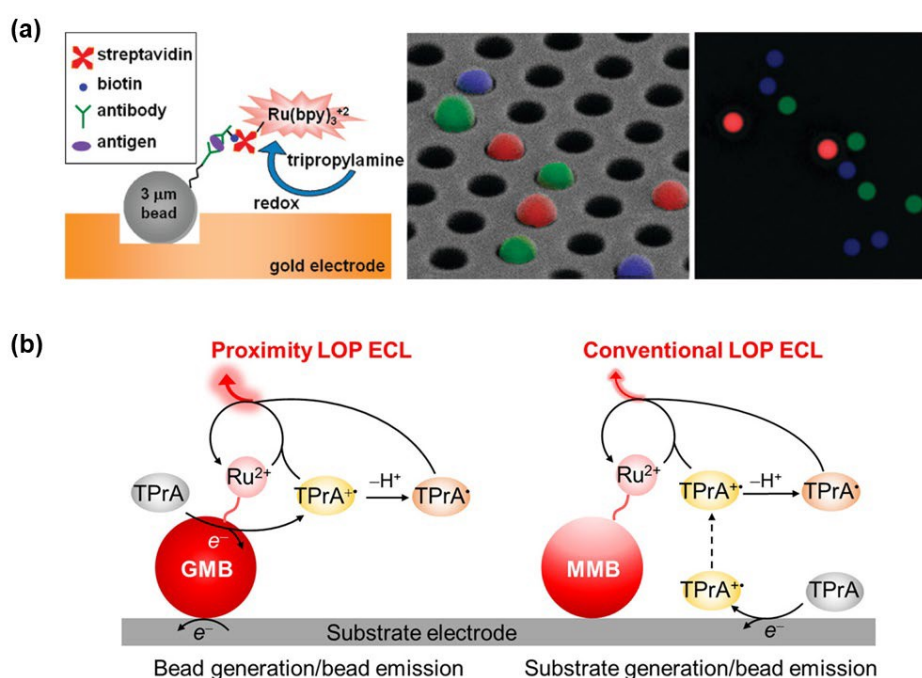


Figure 6. (a) Schematic of bead-based multiplexed ECL immunoassay using $\text{Ru}(\text{bpy})_3^{2+}/\text{TPrA}$ system with spatial resolution. Reprinted with permission from Ref 62. Copyright 2009 American Chemical Society. (b) Comparison of ECL generation efficiency between GMBs and MMBs under different pathways. Reprinted with permission from Ref 63. Copyright 2023 American Chemical Society.

As previously reported, the main limitation in conventional bead-based ECL immunoassays originates from the low oxidation potential pathway.⁴⁰ Because the ECL-emitting region around the bead is determined by the diffusion distance of $\text{TPrA}^{\bullet+}$, and its lifetime is only 0.2 ms, ECL generation is thus limited to a zone within 3 μm of the substrate electrode surface. To overcome this constraint, gold-coated microbeads



(GMBs) were employed as conductive carriers and for constructing proximity ECL generation (**Figure 6b**). As demonstrated, GMBs can function as spherical ultramicroelectrodes for direct coreactant oxidation on their surface, and thus shortening radical diffusion distances and enhancing ECL signals. When using CRP as a model analyte, GMB-based ECL immunoassay achieved a 4.96-fold increase in ECL intensity and a 21.7-fold enhancement in turnover frequency over conventional magnetic microbeads, consequently improving the detection limit from 0.35 ng/mL to 0.12 ng/mL. Moreover, because the ECL generation at GMBs is no longer restricted by the diffusion distance of TPrA^{•+}, the size-encoded multiplex immunoassay is eventually established for four AMI biomarkers, namely CRP, cTnI, FABP, and Myo.⁶³

As discussed above, the spatially-resolved strategy can be implemented using planar microarrays, microfluidic chip, or encoded bead-based microarray. **Table 2** summarizes representative spatially resolved multiplexed ECL immunoassays, detailing their spatial encoding principles, multiplexing capacity, key innovations, detection performance, and commercial availability. These platforms enable multiplexing ranging from dual-plex to eight-plex detection, and exhibit a sensitivity improvement of several orders of magnitude over conventional ELISA, with detection limits reaching fg/mL levels.



Table 2. Summary of representative spatial-resolved ECL immunoassay, detailing the spatial encoding principles, multiplexing capacity, innovations, detection performance, and commercial availability.

Technology Platform	Multiplexing Capacity	Key Innovation	Detection Performance	Commercial Availability	Ref
Spatially Resolved ECL Immunoassay	3-plex (2 panels of biomarkers)	Low-cost 3D-printed chip, physical isolation of detection zones	1-33 pg/mL, cross-reactivity < 6%	Partially available	57
Screen-Printed Electrode Array	3-plex	Portable ECL reader suitable for POC settings	GFAP: 6.94 pg/mL, h-FABP: 1.35 pg/mL, S100 β : 15.73 pg/mL	Fully available	58
Triplex Diagnostic Microchip	3-plex	Chemiluminescence immuno-gold nanoassemblies (ciGold)	0.014-0.053 ng/L, clinical validation showed 100% sensitivity	Partially available	59
3D-Printed Microfluidic Array	8-plex	Automated integration of 3D-printed microfluidic chip	78-110 fg/mL, completed in 25 minutes	Partially available	60
ECLipse Platform	8-plex	Separation of biorecognition and signal generation regions using bipolar electrodes	15-230 fg/mL, sensitivity increased by 7000-fold	Partially available	61
Bead-based Array	Multiplex (variable)	Single-bead-level ECL imaging, fluorescence encoding for bead identification	Single-molecule-level sensitivity	Fully available	62



Gold Microbead-encoded Platform	4-plex	Proximity ECL, spherical ultramicroelectrodes generating reactive radicals autonomously	CRP: 0.12 ng/mL	Fully available	63
Ultra-sensitive Microfluidic Immunoarray	4-plex	Streptavidin-poly-HRP signal amplification	0.013-0.13 fg/mL, dynamic range spanning five orders of magnitude	Partially available	64
CRISPR-ECL Array	3-plex	Integration of CRISPR/Cas13a system with 3D-printed microfluidic array	Sub-fg/mL level sensitivity	Partially available	65
Spatial-Potential Resolved BPE-ECL System	2-plex	Non-precious metal electrocatalyst CuHCF for signal amplification	miRNA-122: 40 fM; CEA: 3 fg/mL	Fully available	66



4. Conclusions and Perspectives

In summary, this review has surveyed recent advances in ECL-based multiplexed immunoassays, with a focus on two primary strategies for achieving multiplex detection, namely, spectrum-resolved strategy and spatial-resolved strategy. The former enables differentiation of multiple targets using multicolor luminophores, such as metal complexes and quantum dots, that emit at distinct wavelengths. The latter achieves multiplexing by physically separating detection sites using microarrays, microfluidic chips, or encoded microbeads. When combined with the ECL imaging technology, this strategy requires only a single ECL luminophore, thus overcoming the limitation of multiplexing capacity imposed by spectral overlap.

Thanks to the remarkable advantages of low background noise, high sensitivity, and high throughput, ECL immunoassays have emerged as a powerful method for multiple biomarker detection in vitro diagnostics and point-of-care testing. Despite significant progress in recent years, some challenges remain to be addressed. For example, although a variety of ECL luminophores have been synthesized, only $\text{Ru}(\text{bpy})_3^{2+}$ and its derivatives have found practical application. This limited selection severely restricts the clinical use of spectrum-resolved multiplexed immunoassays. In addition, numerous innovative ECL assays based on spectrum- and/or spatial-resolved strategies have been established at the methodological level, their validation using real samples containing complex matrices remains limited. Furthermore, standardized protocols for multiplexed ECL immunoassays are still lacking.

Future efforts should focus on improving the spatiotemporal resolution of ECL detection that offers a promising pathway to significantly improve analysis speed in multiplexed immunoassays. Nowadays, electron multiplying charge coupled device (EMCCD) enables high-speed and real-time imaging of ECL emissions from single entities, while achieving microsecond temporal resolution and spatial resolution down to tens of nanometer.^{67,68} However, the imaging time for ECL immunoassays typically ranges from seconds to minutes. Achieving rapid signal acquisition would substantially reduce total assay time, which is a critical improvement for time-sensitive applications



such as emergency diagnostics and point-of-care testing.

View Article Online
DOI: 10.1039/D5SD00236B

On the other hand, the application of artificial intelligence to ECL imaging and spectral analysis offers new opportunities for improving detection accuracy. Machine learning algorithms can assist in identifying spatial features, discriminating signals from background noise, and resolving overlapping emission spectra from multiple luminophores, thereby enabling reliable quantification. The combination of high-speed spatiotemporal imaging with intelligent data processing is expected to advance multiplexed ECL immunoassays toward rapid point-of-care testing, higher throughput, improved sensitivity and specificity, and greater automation.

Author Contributions

Y. Liu: writing – original draft, investigation, visualization, writing – review & editing; C. Liu: writing – original draft, investigation, investigation; Z. Dai: supervision, project administration; W. Guo: writing – review and editing, supervision, project administration, funding acquisition. All authors have read and agreed to the published version of the manuscript.

Conflict of Interest

The authors declare no conflict of interest.

Acknowledgements

This work was financially supported by the Qing Lan Project of Jiangsu Province of China, and the National Natural Science Foundation of China (22522405 and 22374078).

Reference

- 1 A. D. Warren, S. T. Gaylord, K. C. Ngan, M. Dumont Milutinovic, G. A. Kwong, S. N. Bhatia and D. R. Walt, *J. Am. Chem. Soc.*, 2014, **136**, 13709–13714.
- 2 A. Roointan, T. Ahmad Mir, S. Ibrahim Wani, Mati-ur-Rehman, K. K. Hussain, B. Ahmed, S. Abraham, A. Savardashtaki, G. Gandomani, M. Gandomani, R. Chinnappan and M. H. Akhtar, *J. Pharm. Biomed. Anal.*, 2019, **164**, 93–103.
- 3 S. Wang, L. Ge, Y. Zhang, X. Song, N. Li, S. Ge and J. Yu, *Lab Chip*, 2012, **12**, 4489–



- 4498.
- 4 W. Miao and A. J. Bard, *Anal. Chem.*, 2004, **76**, 7109–7113.
 - 5 J. Tian, L. Zhou, Y. Zhao, Y. Wang, Y. Peng and S. Zhao, *Talanta*, 2012, **92**, 72–77.
 - 6 B. S. Munge, T. Stracensky, K. Gamez, D. DiBiase and J. F. Rusling, *Electroanalysis*, 2016, **28**, 2644–2658.
 - 7 P. S. Pakchin, S. A. Nakhjavani, R. Saber, H. Ghanbari and Y. Omid, *TrAC Trends Anal. Chem.*, 2017, **92**, 32–41.
 - 8 R. Liu, S. Zhang, C. Wei, Z. Xing, S. Zhang and X. Zhang, *Acc. Chem. Res.*, 2016, **49**, 775–783.
 - 9 Z. Yang, C. Zong, F. Yan and H. Ju, *Talanta*, 2010, **82**, 1462–1467.
 - 10 S. Otsuki and M. Ishikawa, *Biosens. Bioelectron.*, 2010, **26**, 202–206.
 - 11 Z. Cao, H. Li, C. Lau and Y. Zhang, *Anal. Chim. Acta*, 2011, **698**, 44–50.
 - 12 J. Li, J. Wang, Y. S. Grewal, C. B. Howard, L. J. Raftery, S. Mahler, Y. Wang and M. Trau, *Anal. Chem.*, 2018, **90**, 10377–10384.
 - 13 Z. Liu, Q. Rong, Z. Ma and H. Han, *Biosens. Bioelectron.*, 2015, **65**, 307–313.
 - 14 W. Miao, *Chem. Rev.*, 2008, **108**, 2506–2553.
 - 15 L. Hu and G. Xu, *Chem. Soc. Rev.*, 2010, **39**, 3275–3304.
 - 16 H. Qi and C. Zhang, *Anal. Chem.*, 2020, **92**, 524–534.
 - 17 M. M. Richter, *Chem. Rev.*, 2004, **104**, 3003–3036.
 - 18 Y. Wang, W. Guo, Q. Yang and B. Su, *J. Am. Chem. Soc.*, 2020, **142**, 1222–1226.
 - 19 R. E. Visco and E. A. Chandross, *J. Am. Chem. Soc.*, 1964, **86**, 5350–5351.
 - 20 F. Kanoufi and A. J. Bard, *J. Phys. Chem. B*, 1999, **103**, 10469–10480.
 - 21 M.-F. Sun, J.-L. Liu, Y.-Q. Chai, J. Zhang, Y. Tang and R. Yuan, *Anal. Chem.*, 2019, **91**, 7765–7773.
 - 22 M. M. Richter, *Chem. Rev.*, 2004, **104**, 3003–3036.
 - 23 K. S. V. Santhanam and A. J. Bard, *J. Am. Chem. Soc.*, 1965, **87**, 139–140.
 - 24 R. E. Visco and E. A. Chandross, *J. Am. Chem. Soc.*, 1964, **86**, 5350–5351.
 - 25 D. L. Maricle and Arthur. Maurer, *J. Am. Chem. Soc.*, 1967, **89**, 188–189.
 - 26 R. Bezman and L. R. Faulkner, *J. Am. Chem. Soc.*, 1972, **94**, 6324–6330.
 - 27 W. Miao, *Chem. Rev.*, 2008, **108**, 2506–2553.
 - 28 P. Bertoncello and R. J. Forster, *Biosens. Bioelectron.*, 2009, **24**, 3191–3200.
 - 29 R. S. Glass and L. R. Faulkner, *J. Phys. Chem.*, 1981, **85**, 1160–1165.
 - 30 R. Pyati and M. M. Richter, *Annu. Rep. Sect. C Phys. Chem.*, 2007, **103**, 12–78.
 - 31 E. L. Ritchie, P. Pastore and R. M. Wightman, *J. Am. Chem. Soc.*, 1997, **119**, 11920–11925.
 - 32 H. S. White and A. J. Bard, *J. Am. Chem. Soc.*, 1982, **104**, 6891–6895.
 - 33 P. J. Smith and C. K. Mann, *J. Org. Chem.*, 1969, **34**, 1821–1826.
 - 34 R. Y. Lai and A. J. Bard, *J. Phys. Chem. A*, 2003, **107**, 3335–3340.
 - 35 R. D. Gerardi, N. W. Barnett and S. W. Lewis, *Anal. Chim. Acta*, 1999, **378**, 1–41.
 - 36 W. Miao, J.-P. Choi and A. J. Bard, *J. Am. Chem. Soc.*, 2002, **124**, 14478–14485.
 - 37 R. Memming, *J. Electrochem. Soc.*, 1969, **116**, 785.
 - 38 R. Qiu, X. Zhang, H. Luo and Y. Shao, *Chem. Sci.*, 2016, **7**, 6684–6688.
 - 39 J. Liu, K. Yu, H. Zhang, J. He, J. Jiang and H. Luo, *Chem. Sci.*, 2021, **12**, 9494–9499.
 - 40 M. Sentic, M. Milutinovic, F. Kanoufi, D. Manojlovic, S. Arbault and N. Sojic, *Chem.*



Sci., 2014, **5**, 2568–2572.

View Article Online
DOI: 10.1039/D5SD00236B

- 41 Y. Wang, W. Guo, Q. Yang and B. Su, *J. Am. Chem. Soc.*, 2020, **142**, 1222–1226.
- 42 Y. Wang, J. Ding, P. Zhou, J. Liu, Z. Qiao, K. Yu, J. Jiang and B. Su, *Angew. Chem. Int. Ed.*, 2023, **62**, e202216525.
- 43 D. Bruce, M. M. Richter and K. J. Brewer, *Anal. Chem.*, 2002, **74**, 3157–3159.
- 44 D. Bruce and M. M. Richter, *Anal. Chem.*, 2002, **74**, 1340–1342.
- 45 W. Guo, H. Ding, C. Gu, Y. Liu, X. Jiang, B. Su and Y. Shao, *J. Am. Chem. Soc.*, 2018, **140**, 15904–15915.
- 46 Z. Guo, T. Hao, S. Du, B. Chen, Z. Wang, X. Li and S. Wang, *Biosens. Bioelectron.*, 2013, **44**, 101–107.
- 47 G. Zou, X. Tan, X. Long, Y. He and W. Miao, *Anal. Chem.*, 2017, **89**, 13024–13029.
- 48 J. Zhou, L. Nie, B. Zhang and G. Zou, *Anal. Chem.*, 2018, **90**, 12361–12365.
- 49 Z. Cao, Y. Shu, H. Qin, B. Su and X. Peng, *ACS Cent. Sci.*, 2020, **6**, 1129–1137.
- 50 L. Yu, M. Li, Q. Kang, L. Fu, G. Zou and D. Shen, *Biosens. Bioelectron.*, 2021, **176**, 112934.
- 51 F. Zhang, Y. He, K. Fu, L. Fu, B. Zhang, H. Wang and G. Zou, *Biosens. Bioelectron.*, 2018, **115**, 77–82.
- 52 J. Ge, J. Dou, X. Yu, Y. Sun, H. Song and D. Shen, *Microchem. J.*, 2024, **199**, 110117.
- 53 Y. Lv, Z. Zhou, Y. Shen, Q. Zhou, J. Ji, S. Liu and Y. Zhang, *ACS Sens.*, 2018, **3**, 1362–1367.
- 54 X. Gao, X. Liu, Y. Zeng, Q. Zhang, B. Zhang and G. Zou, *Anal. Chem.*, 2022, **94**, 15801–15808.
- 55 J. D. Hoheisel, *Nat. Rev. Genet.*, 2006, **7**, 200–210.
- 56 Y. Zhang, W. Liu, S. Ge, M. Yan, S. Wang, J. Yu, N. Li and X. Song, *Biosens. Bioelectron.*, 2013, **41**, 684–690.
- 57 M. Jović, D. Prim, G. Paciotti and M. E. Pfeifer, *Lab Chip*, 2025, **25**, 5428–5438.
- 58 M. Jović, D. Prim, E. Saini and M. E. Pfeifer, *Biosensors*, 2022, **12**, 172.
- 59 M. Guo, D. Du, J. Wang, Y. Ma, D. Yang, M. A. Haghghatbin, J. Shu, W. Nie, R. Zhang, Z. Bian, L. Wang, Z. J. Smith and H. Cui, *Chem. Biomed. Imaging*, 2023, **1**, 179–185.
- 60 K. Kadimisetty, S. Malla, K. S. Bhalerao, I. M. Mosa, S. Bhakta, N. H. Lee and J. F. Rusling, *Anal. Chem.*, 2018, **90**, 7569–7577.
- 61 Y. K. Cho, H. Kim, A. Bénard, H.-K. Woo, F. Czubyko, P. David, F. J. Hansen, J. I. Lee, J. H. Park, E. Schneck, G. F. Weber, I.-S. Shin and H. Lee, *Sci. Adv.*, 2022, **8**, eabq4022.
- 62 F. Deiss, C. N. LaFratta, M. Symer, T. M. Blicharz, N. Sojic and D. R. Walt, *J. Am. Chem. Soc.*, 2009, **131**, 6088–6089.
- 63 X. Yang, J. Hang, W. Qu, Y. Wang, L. Wang, P. Zhou, H. Ding, B. Su, J. Lei, W. Guo and Z. Dai, *J. Am. Chem. Soc.*, 2023, **145**, 16026–16036.
- 64 L. Dhanapala, A. L. Jones, P. Czarnecki and J. F. Rusling, *Anal. Chem.*, 2020, **92**, 8021–8025.
- 65 K. Hiniduma, P. I. T. De Silva, R. Canete, P. Vora, H. Gunathillaka, O. Clement, S. M. Shawky, J. L. Rouge, I. M. Mosa, D. C. Steffens, K. Manning, D. Breno and J. F. Rusling, *Biosens. Bioelectron.*, 2025, **289**, 117855.



- 66 H. Li, Q. Cai, Z. Li, G. Jie and H. Zhou, *Biosens. Bioelectron.*, 2024, **255**, 116258. View Article Online
DOI:10.1039/D5SD00236B
- 67 J. Dong, Y. Lu, Y. Xu, F. Chen, J. Yang, Y. Chen and J. Feng, *Nature*, 2021, **596**, 244–249.
- 68 D. Ye, Y.-C. Kong, C.-H. Xu, Z. Ma, Y. Xiong, H. Zhao and W. Zhao, *J. Am. Chem. Soc.*, 2026, DOI:10.1021/jacs.5c18188.



Data Availability Statement

View Article Online
DOI: 10.1039/D5SD00236B

No primary research results, software or code have been included and no new data were generated or analysed as part of this review.

